

# NH<sub>3</sub> in the Central 10 pc of the Galaxy. II. Determination of Opacity for Gas with Large Linewidths

Robeson S. McGary<sup>1</sup> and Paul T.P. Ho<sup>1</sup>

## ABSTRACT

The 23 GHz emission lines from the NH<sub>3</sub> rotation inversion transitions are widely used to investigate the kinematics and physical conditions in dense molecular clouds. The line profile is composed of hyperfine components which can be used to calculate the opacity of the gas (Ho & Townes 1983). For intrinsic linewidths of a few km s<sup>-1</sup>, the 18 magnetic hyperfine components blend together to form a line profile composed of five quadrupole hyperfine lines. If the intrinsic linewidth exceeds one half of the separation of these quadrupole hyperfine components ( $\sim 5 - 10$  km s<sup>-1</sup>) these five lines blend together and the observed linewidths greatly overestimate the intrinsic linewidths. If uncorrected, these artificially broad linewidths will lead to artificially high opacities. We have observed this effect in our NH<sub>3</sub> data from the central 10 pc of the Galaxy where uncorrected NH<sub>3</sub>(1,1) linewidths of  $\sim 30$  km s<sup>-1</sup> exaggerate the intrinsic linewidths by more than a factor of two (Genzel & Townes 1987). Models of the effect of blending on the line profile enable us to solve for the intrinsic linewidth and opacity of NH<sub>3</sub> using the observed linewidth and intensity of two NH<sub>3</sub> rotation inversion transitions. By using the observed linewidth instead of the entire line profile, our method may also be used to correct linewidths in historical data where detailed information on the shape of the line profile is no longer available. We present the result of the application of this method to our Galactic Center data. We successfully recover the intrinsic linewidth ( $\langle \Delta v_{\text{int}} \rangle \approx 15$  km s<sup>-1</sup>) and opacity of the gas. Clouds close to the nucleus in projected distance as well as those that are being impacted by Sgr A East show the highest intrinsic linewidths. The cores of the “southern streamer” (Ho et al. 1991; Coil & Ho 1999, 2000) and the “50 km s<sup>-1</sup>” giant molecular cloud (GMC, Güsten, Walmsley, & Pauls (1981)) have the highest opacities.

---

<sup>1</sup>Harvard-Smithsonian Center for Astrophysics, 60 Garden Street, Cambridge, MA 02138, [rmcgary@cfa.harvard.edu](mailto:rmcgary@cfa.harvard.edu), [pho@cfa.harvard.edu](mailto:pho@cfa.harvard.edu)

## 1. Introduction

The metastable ( $J=K$ ) rotation inversion transitions of  $\text{NH}_3$  are effective tracers of dense molecular material ( $N_{\text{H}} \approx 10^4 - 10^5 \text{ cm}^{-3}$ ) (Ho & Townes 1983). The  $\text{NH}_3$  rotation inversion transitions are most often used to trace dense cores of giant molecular clouds (GMCs), but they are also observed in the “streamers” near the Galactic Center (Ho et al. 1991; Coil & Ho 1999, 2000; McGary et al. 2001) which will be our example data for this paper. With frequencies near 23 GHz (1.3 cm), these transitions are easily observable with radio telescopes such as the Very Large Array<sup>2</sup> (VLA) with only minimal interference by the atmosphere. Compared to high frequency tracers such as the 3 mm transitions of  $\text{HCN}(J=1-0)$  and  $\text{HCO}^+(J=1-0)$  which often have  $\tau > 1$ , these  $\text{NH}_3$  transitions tend to be more optically thin, even in the case of low temperatures. As a result, spectra of  $\text{NH}_3$  rotation inversion transitions are usually free of self-absorption effects.

The  $\text{NH}_3$  rotation inversion line is composed of 18 magnetic hyperfine lines which are grouped into five main features (a detailed description of the  $\text{NH}_3$  rotation inversion transitions can be found in Townes & Schalow (1975) and Ho & Townes (1983)). The spacing of the magnetic hyperfine lines within each of the five components is too close to resolve except in cool and quiescent dense cores where the intrinsic linewidths of the gas can be less than  $1 \text{ km s}^{-1}$ . The effect of blending of the 18 magnetic hyperfine components on the observed linewidth is discussed in detail in Ho et al. (1977) and Barranco & Goodman (1998). For linewidths of a few  $\text{km s}^{-1}$ , the magnetic hyperfine components within each of the five features will blend together to form five electric quadrupole hyperfine components consisting of a main line and two symmetric pairs of satellite lines. In this paper, we focus on large intrinsic linewidths and therefore will only concern ourselves with this “five-peak” profile. These quadrupole satellite lines are located from 10 to  $30 \text{ km s}^{-1}$  from the main line (see Table 1 for relative spacings and intensities). Comparison of the intensity of a satellite line to the main line enables a direct calculation of the opacity of the gas making the  $\text{NH}_3$  rotation inversion transitions especially useful. The derived opacity can then be used to calculate  $N_{\text{H}}$ , masses, and also combined with line ratios of different transitions to determine the rotational temperature of the gas (Ho & Townes 1983).

The small frequency separation of the five quadrupole hyperfine lines means that for large intrinsic linewidths,  $\Delta v_{\text{int}}$ , the satellite and main hyperfine components will be blended into a single line. Figure 1 shows line profiles for  $\text{NH}_3(1,1)$  for a range of intrinsic linewidths for  $\tau_{\text{m}} \ll 1$ . For  $\Delta v_{\text{int}} \gtrsim 5 \text{ km s}^{-1}$  the five components are blended into a single profile

---

<sup>2</sup>The National Radio Astronomy Observatory is a facility of the National Science Foundation operated under cooperative agreement by Associated Universities, Inc.

and it becomes difficult to measure the relative intensities needed for opacity estimation. The situation is aggravated by the fact that an increase in opacity will result in an increase in the intensity of the satellite hyperfine lines relative to the main line and the blended profile will appear to broaden even more. As a result, an increase in either  $\tau_m$  or  $\Delta v_{\text{int}}$  will appear as an increase in the observed linewidth,  $\Delta v_{\text{obs}}$ , and it is difficult to interpret the data. Exaggerated estimates of opacity as a result of mis-fitting intrinsically broad lines can greatly limit the physical parameters that can be determined from the data. For example, if  $\text{NH}_3(1,1)$  gas has  $\Delta v_{\text{int}} > 5 \text{ km s}^{-1}$ , then an increase in linewidth may be mistaken as an increase in opacity. The overestimation of the opacity propagates into overestimations of the column density and ultimately the calculated mass of the gas. In the case of our Galactic Center data, the observed linewidths are high and the challenge is to determine the extent of the contribution from shocked material with large intrinsic linewidths as well as that from high opacity gas. Shocks are important for identifying the locations of possible interactions between the streamers of molecular material that surround the Galactic Center. A mistaken calculation of the mass of a cloud or incorrect identification of a shock could affect our general understanding of the environment in the central parsecs of the Galaxy. It is therefore obvious that we need an improved method to obtain independent estimates of the opacity and intrinsic linewidth of the gas.

In this paper, we present a method to disentangle the effects of large intrinsic linewidths and high opacities by comparing the observed linewidths and intensities of two  $\text{NH}_3$  transitions. Because the exact shape of the line profile need not be known, this method can be easily applied to historical data where the line profiles are no longer available. Throughout the paper, we combine the theoretical discussion with a test case example using our  $\text{NH}_3(1,1)$ ,  $(2,2)$ , and  $(3,3)$  data from the Galactic Center. In §2, we show the correlation between  $\Delta v_{\text{obs}}$  and  $\tau_m$  in our Galactic Center data when the two quantities are solved for in the traditional manner. Section 3.1 then presents a calculation of the dependence of  $\Delta v_{\text{obs}}$  on  $\Delta v_{\text{int}}$  for  $\text{NH}_3(1,1)$ ,  $(2,2)$ , and  $(3,3)$  for the special case where  $\tau_m \ll 1$ . This is followed by the incorporation of variations in opacity. The full method for simultaneously solving for the opacity and intrinsic linewidth is presented in §4. The paper concludes by presenting the maps of the best estimate of  $\Delta v_{\text{int}}$  and  $\text{NH}_3(1,1)$  opacity for our Galactic Center data. The map of intrinsic linewidths shows  $\langle \Delta v_{\text{int}} \rangle = 15 \text{ km s}^{-1}$  for  $\text{NH}_3(1,1)$  which is in agreement with observations of other tracers. In addition, the corrected opacities show that all except the most massive features in the map are optically thin. The opacity and intrinsic linewidths of the observed features are then discussed.

## 2. The Observed Correlation between $\Delta v_{\text{obs}}$ and $\tau_m$

Gas near the Galactic center has been observed to have intrinsic linewidths of 10–20 km s<sup>-1</sup>, and therefore provides a good test of the effects of blending of hyperfine lines on the calculation of the opacity (Güsten & Downes 1980; Armstrong & Barrett 1985). We observed the central 10 pc of the Galaxy in NH<sub>3</sub>(1,1), (2,2), and (3,3) in 1999 March (McGary et al. 2001). The data were taken at 23 GHz in the D-northC configuration of the Very Large Array (VLA) to provide the largest and most circular beam possible. A Gaussian taper was applied to the  $uv$  data resulting in a synthesized beam of 15'' × 13'', which is useful for detection of extended features in our maps. The data have a velocity coverage of ±150 km s<sup>-1</sup>, which includes almost all detected motions at the Galactic Center, and a velocity resolution of 9.8 km s<sup>-1</sup>. In addition, a five pointing mosaic ensures full spatial coverage of the region. We choose the rotation inversion transitions of NH<sub>3</sub> so that we can directly use the hyperfine lines to calculate the opacity of the gas. The opacity is then combined with line ratios to calculate the rotational temperature of features observed in the central 10 pc (Ho & Townes 1983). Increased temperatures can be a sign of shocked gas which is important in determining if there are cloud-cloud collisions or shocks from the expanding supernova remnant, Sgr A East (Genzel et al. 1990; Ho et al. 1991; Serabyn, Lacy, & Achtermann 1992; Zylka 1999). Accurate measurements of the intrinsic linewidth of the gas are also important for locating shocked regions. The large photon flux from the nucleus may also heat gas, and features close to the Galactic Center should appear warmer. All of these quantities depend on accurate measurements of the opacity and intrinsic linewidth of the gas.

We initially solved for the opacity in the traditional manner by comparing the flux density of the main component to the average flux density of the two outermost hyperfine components (±19.3 km s<sup>-1</sup> for NH<sub>3</sub>(1,1)). By averaging these two lines, we increase the S/N by a factor of  $\sqrt{2}$  and opacities are only calculated where this average hyperfine flux density is greater than  $3/\sqrt{2}\sigma_{\text{JK}}$  where  $\sigma_{11} = 0.009$  Jy Beam<sup>-1</sup>,  $\sigma_{22} = 0.009$  Jy Beam<sup>-1</sup>, and  $\sigma_{33} = 0.011$  Jy Beam<sup>-1</sup>. From radiative transfer, the opacity is related to the observed flux density of the main and satellite hyperfine lines by

$$\frac{S(\nu)_m}{S(\nu)_s} = \frac{[\Delta T_A(\nu)]_m}{[\Delta T_A(\nu)]_s} = \frac{1 - e^{-\tau(\nu)_m}}{1 - e^{-a\tau(\nu)_m}} \quad (1)$$

where  $S(\nu)_m$  and  $S(\nu)_s$  refer to flux densities of the main and satellite lines,  $[\Delta T_A(\nu)]_m$  and  $[\Delta T_A(\nu)]_s$  are the respective antenna temperatures,  $\tau(\nu)_m$  is the opacity of the main hyperfine component, and  $a$  is the theoretical intensity of the satellite line compared to the main line for  $\tau(\nu) \ll 1$ . Note that this equation assumes equal beam filling factors and excitation temperatures for the two transitions. The theoretical relative intensities of the

quadrupole satellite hyperfine lines for  $\text{NH}_3(1,1)$ ,  $(2,2)$ , and  $(3,3)$  are listed in Table 1.

Meanwhile, an observed linewidth,  $\Delta v_{\text{obs}}$  (defined in this paper as the FWHM), is fit to every pixel in the map by fitting a Gaussian of the form

$$f(v) = A_0 e^{-\frac{(v-v_0)^2}{2\sigma_{\text{obs}}^2}} \quad (2)$$

where  $v_0$  is the peak velocity at each position and  $\Delta v_{\text{obs}} = 2.35\sigma_{\text{obs}}$ . Observed linewidths are only calculated for pixels where the peak flux in the channel corresponding to  $v_0$  is greater than  $3\sigma_{\text{JK}}$ . The calculated observed linewidths are also required to be less than  $100 \text{ km s}^{-1}$ . The  $\text{NH}_3(1,1)$  data give  $\langle \Delta v_{\text{obs}} \rangle = 30 \text{ km s}^{-1}$  which is approximately a factor of two larger than what is observed in other tracers (Güsten & Downes 1980; Armstrong & Barrett 1985; Genzel & Townes 1987). Linewidths calculated from the  $\text{NH}_3(3,3)$  data, however, have  $\langle \Delta v_{\text{obs}} \rangle = 18 \text{ km s}^{-1}$ . For  $\tau_{\text{m}} \ll 1$ , the  $\text{NH}_3(1,1)$  satellite hyperfine lines are a much larger fraction of the main line intensity (28 and 22%) than in the case of  $\text{NH}_3(3,3)$  ( $\sim 3\%$ ). In addition, the  $\text{NH}_3(1,1)$  quadrupole hyperfine lines have a much smaller velocity separation than the higher transitions (see Table 1). These two characteristics of  $\text{NH}_3(1,1)$  make it much more susceptible to corruption by blending of the quadrupole hyperfine lines at large intrinsic linewidths. The difference in the observed linewidths for the  $\text{NH}_3(1,1)$  and  $(3,3)$  data may thus be explained by the large intrinsic linewidths near the Galactic Center.

To test whether blending has affected the  $\text{NH}_3(1,1)$  data, we plot  $\Delta v_{\text{obs}}$  as a function of the main line opacity,  $\tau_{\text{m}}(1,1)$  for every pixel in our  $\text{NH}_3(1,1)$  map where  $\Delta v_{\text{obs}} < 100 \text{ km s}^{-1}$  and  $\tau_{\text{m}}(1,1) < 5$  (see Figure 2a). The main line opacity has been calculated using Equation 1 and the relative intensities of the main and outer satellite hyperfine lines. The noise in one channel,  $\sigma_{11}$ , results in an estimated error of  $\sim 0.1$  for  $\tau_{\text{m}}(1,1)$ . The error in  $\Delta v_{\text{obs}}$  is  $1\text{--}2 \text{ km s}^{-1}$  (see §4.1). A strong correlation between the two quantities is observed. However, there are many pixels per  $\sim 15''$  beam resulting in correlation between adjacent pixels. In Figure 2b, we average over the beam and sample once per beam resulting in independent pixels. The correlation coefficient between  $\Delta v_{\text{obs}}$  and  $\tau_{\text{m}}(1,1)$  is 0.69. Figure 3 shows the same parameters for  $\text{NH}_3(3,3)$  and the correlation coefficient between  $\Delta v_{\text{obs}}$  and  $\tau_{\text{m}}(3,3)$  is only 0.07. The fact that the correlation is weaker in  $\text{NH}_3(3,3)$  than  $(1,1)$  suggests that the correlation between  $\Delta v_{\text{obs}}$  and  $\tau_{\text{m}}(1,1)$  is not real, but is an artifact of blending of the hyperfine components. It is interesting to note that there are no points with  $\tau_{\text{m}}(3,3) < 1.0$  in this figure. This effect is explained by the minimum flux cutoff of  $3\sigma_{33}$  ( $0.03 \text{ Jy beam}^{-1}$ ) required for the average outer satellite hyperfine line. Because the satellite hyperfine lines are intrinsically weaker in  $\text{NH}_3(3,3)$  than in  $(1,1)$  (see Table 1), the  $(3,3)$  hyperfine lines are often below this noise cutoff resulting in an effective cutoff in the minimum  $\tau_{\text{m}}(3,3)$  to which we are sensitive.

### 3. Dependence of $\Delta v_{\text{obs}}$ on $\Delta v_{\text{int}}$ and $\tau_m$

In order to develop a method to remove the effects of blending on  $\Delta v_{\text{obs}}$ , we must model the dependence of the observed linewidth on both the intrinsic linewidth and the opacity of the gas. The opacity of the gas as a function of velocity is defined as

$$\tau(v) = \tau_m \phi(v, \sigma) \quad (3)$$

where  $\tau_m$  is the opacity at the center of the main line and  $\phi(v, \sigma)$  is the normalized line profile for the rotation inversion transition. The quadrupole hyperfine components are modeled by five Gaussians with velocity spacings and relative intensities of the satellite hyperfine lines defined as in Table 1. The profile is written explicitly as

$$\begin{aligned} \phi(v, \sigma) = & e^{-v^2/2\sigma_{\text{int}}^2} \\ & + a_{\text{in}} e^{-(v-\Delta v_{\text{in}})^2/2\sigma_{\text{int}}^2} + a_{\text{in}} e^{-(v+\Delta v_{\text{in}})^2/2\sigma_{\text{int}}^2} \\ & + a_{\text{out}} e^{-(v-\Delta v_{\text{out}})^2/2\sigma_{\text{int}}^2} + a_{\text{out}} e^{-(v+\Delta v_{\text{out}})^2/2\sigma_{\text{int}}^2} \end{aligned} \quad (4)$$

where  $\sigma_{\text{int}} = \Delta v_{\text{int}}/2.35$  is the standard deviation of the line profile,  $\Delta v_{\text{in}}$  and  $\Delta v_{\text{out}}$  are the offsets of the inner and outer satellite hyperfine lines (in  $\text{km s}^{-1}$ ) respectively, and  $a_{\text{in}}$  and  $a_{\text{out}}$  are the intensities of the inner and outer satellite hyperfine lines assuming an intensity of 1.0 for the main line (see Table 1). The intensity of the line is given by

$$I(v, \sigma, \tau_m) = (T_{\text{ex}} - T_{\text{b}})[1 - e^{-\tau_m \phi(v, \sigma)}] . \quad (5)$$

Throughout the paper, when the opacity is referred to in the general case, we use  $\tau_m$ . For a specific (J,K) transition of  $\text{NH}_3$ , the main line opacity is written as  $\tau_m(\text{J,K})$ . It is this opacity of the main line,  $\tau_m$ , that is reported in most observational papers and in keeping with this convention, the opacities derived in this paper all refer to  $\tau_m$ .

#### 3.1. Dependence of $\Delta v_{\text{obs}}$ on $\Delta v_{\text{int}}$ for $\tau_m \ll 1$

We begin by calculating the line profile as a function of  $\Delta v_{\text{int}}$  in the special case where  $\tau_m \ll 1$ . We need not be concerned with the observed value of  $I(v, \sigma, \tau_m)$  because the FWHM and relative intensity of the main and satellite hyperfine lines are independent of the absolute amplitude of the line. Therefore, Equation 5 reduces to  $I(v, \sigma, \tau_m) \propto \phi(v, \sigma)$  for  $\tau_m \ll 1$ .

Figure 1 compares the line profiles of  $\text{NH}_3(1,1)$  for  $\tau_m \ll 1$  for a range of intrinsic linewidths. For  $\Delta v_{\text{int}} \gtrsim 5 \text{ km s}^{-1}$ , the main and satellite components of  $\text{NH}_3(1,1)$  blend into a single line profile and fitting a Gaussian profile to the main component will overestimate the intrinsic linewidth of the gas.

In order to determine  $\Delta v_{\text{obs}}$  as a function of  $\Delta v_{\text{int}}$  for  $\text{NH}_3(1,1)$ ,  $(2,2)$ , and  $(3,3)$ , normalized line profiles as a function of  $\Delta v_{\text{int}}$  and  $v$  are generated for the case where  $\tau_m \ll 1$ . For each normalized line profile, a Gaussian is fit to the main component to determine the resulting observed linewidth. By modeling the effect of  $\Delta v_{\text{int}}$  and  $\tau_m$  on the observed linewidth, the method for recovering the intrinsic linewidth can be applied to any historical data where the entire line profile may no longer be available. Figure 4a shows  $\Delta v_{\text{obs}}$  as a function of  $\Delta v_{\text{int}}$  for  $\text{NH}_3(1,1)$ ,  $(2,2)$ , and  $(3,3)$  assuming  $\tau_m \ll 1$ . For  $\Delta v_{\text{int}} \lesssim 5 \text{ km s}^{-1}$ , no blending occurs and all three transitions have  $\Delta v_{\text{obs}} \approx \Delta v_{\text{int}}$ . Note that we are not concerned with the case of dark cores where intrinsic linewidths of only a few  $\text{km s}^{-1}$  cause the closely separated 18 magnetic hyperfine lines to blend, which is discussed in detail in Ho et al. (1977) and Barranco & Goodman (1998).

For intrinsic linewidths greater than  $5 \text{ km s}^{-1}$ , the satellite hyperfine lines of  $\text{NH}_3(1,1)$  blend with the main line and  $\Delta v_{\text{obs}}(1,1)$  will greatly exaggerate  $\Delta v_{\text{int}}$  for  $\Delta v_{\text{int}} \gtrsim 5 \text{ km s}^{-1}$ , *independent of opacity and velocity resolution*.  $\text{NH}_3(2,2)$  and  $(3,3)$  give a much better estimation of the intrinsic linewidth for  $\tau_m \ll 1$  because the satellite hyperfine lines are relatively weaker compared to the main lines and are also located further from the main line than in the case of  $\text{NH}_3(1,1)$ . In our Galactic Center data, we find  $\langle \Delta v_{\text{obs}} \rangle = 30 \text{ km s}^{-1}$  for  $\text{NH}_3(1,1)$  and  $\langle \Delta v_{\text{obs}} \rangle = 18 \text{ km s}^{-1}$  for  $\text{NH}_3(3,3)$ . These results can be fit almost exactly by  $\Delta v_{\text{int}} = 17 \text{ km s}^{-1}$  in Figure 4a.

Figure 4b plots  $\Delta v_{\text{obs}}/\Delta v_{\text{int}}$  for intrinsic linewidths up to  $60 \text{ km s}^{-1}$ . For each transition, there exists a velocity,  $v_{\text{crit}}$ , above which the exaggeration of  $\Delta v_{\text{int}}$  by  $\Delta v_{\text{obs}}$  decreases. As the intrinsic linewidths approach  $v_{\text{crit}}$ , the line profile is broadening as the satellite hyperfine lines blend with the main line. However, once the intrinsic linewidth of the gas is greater than the maximum separation of the hyperfine lines, the effect of the satellite hyperfine lines on  $\Delta v_{\text{obs}}$  becomes less important and  $\Delta v_{\text{obs}}$  asymptotically approaches  $\Delta v_{\text{int}}$ . The critical velocities for  $\text{NH}_3(1,1)$ ,  $(2,2)$ , and  $(3,3)$  are 8, 20, and  $27 \text{ km s}^{-1}$ , respectively. For the Galactic Center where  $\Delta v_{\text{int}} \approx 15 \text{ km s}^{-1}$ ,  $\text{NH}_3(1,1)$  gives by far the worst overestimation of  $\Delta v_{\text{int}}$ . However, for  $\Delta v_{\text{int}} \gtrsim 50 \text{ km s}^{-1}$ ,  $\text{NH}_3(2,2)$  is equally as bad as  $\text{NH}_3(1,1)$ . For the remainder of this paper, we focus on  $\Delta v_{\text{int}} \leq 30 \text{ km s}^{-1}$ , as expected at the Galactic Center.

### 3.2. Observed line profiles as a function of $\Delta v_{\text{int}}$ and $\tau$

In this section, we calculate line profiles for the case where the opacity is large enough that the intensity of the satellite hyperfine lines becomes important. In the case of the blended profile, an increase in opacity will appear as an increase in the observed linewidth of the profile. Figures 1 and 5 can be used to compare the effects of changes in either  $\Delta v_{\text{int}}$  or  $\tau_m$  while the other parameter is held constant. As seen in Figure 1, an increase in  $\Delta v_{\text{int}}$  for constant opacity results in broadening of the line profile until the five quadrupole hyperfine lines blend together. Figures 5a and 5b show the effect of varying  $\tau_m$  when  $\Delta v_{\text{int}} = 3$  and  $15 \text{ km s}^{-1}$  for  $\text{NH}_3(1,1)$ . In Figure 5a,  $\Delta v_{\text{int}} < 5 \text{ km s}^{-1}$  so the profiles are not blended. As a result, an increase in  $\tau_m$  only results in an increase in the relative intensities of the satellite lines with respect to the main line. In Figure 5b, however, the blended profile appears to broaden dramatically as the opacity is increased.

Using the definition of the line profile in Equation 5, an array of line profiles is generated for a range of opacities and intrinsic linewidths. If the data have good velocity resolution with many channels across the profile, then the intrinsic linewidth and  $\tau_m$  of any  $\text{NH}_3$  rotation inversion transition may be solved for without any additional information from other tracers. In this case, a least squares minimization routine can be used to search this array to find the  $\Delta v_{\text{int}}$  and  $\tau_m$  that give the best fit to the observed line profile. In the case where multiple transitions of  $\text{NH}_3$  are observed, similar results may be easily obtained by comparing only the observed linewidths and intensities of the lines. For each line profile in the generated data, the main line is fit with a Gaussian to estimate the expected value for  $\Delta v_{\text{obs}}$ . Figure 6 shows the dependence of  $\Delta v_{\text{obs}}$  on  $\Delta v_{\text{int}}$  and  $\tau_m$  for the simulated  $\text{NH}_3(1,1)$ ,  $(2,2)$ , and  $(3,3)$  data. For small intrinsic linewidths, the hyperfine components are well-separated and  $\Delta v_{\text{obs}} \approx \Delta v_{\text{int}}$ , independent of  $\tau_m$ . A discontinuity develops near  $5 \text{ km s}^{-1}$  for  $\text{NH}_3(1,1)$  and  $8 \text{ km s}^{-1}$  for  $\text{NH}_3(2,2)$  in the optically thick cases resulting from the blending of main and satellite hyperfine components with comparable intensities (see the line profile for  $\tau_m(1,1) = 5.0$  in Figure 5a).  $\text{NH}_3(3,3)$  does not show this effect in our models because the satellite hyperfine lines are  $< 20\%$  of the intensity of the main component even in the case where  $\tau_m(3,3) = 5.0$ . Using Figure 6a, we find that for an average intrinsic linewidth at the Galactic Center data of  $17 \text{ km s}^{-1}$  as in §3.1, the average observed linewidth of  $30 \text{ km s}^{-1}$  in our data indicates that  $0.01 < \tau_m(1,1) < 1.0$ .

### 4. Method to Simultaneously Determine $\Delta v_{\text{int}}$ , $\tau_m(1,1)$ , and $\tau_m(3,3)$

In this section, we outline the detailed steps of our method for recovering the intrinsic linewidths and opacities of gas with large linewidths using our Galactic Center data as an



example. We use  $\text{NH}_3$  (1,1) and (3,3) because they are the brightest tracers in our data and thus have the most points for which  $\Delta v_{\text{obs}}$  can be calculated for both transitions. There is much  $\text{NH}_3$ (1,1) emission because it traces the lowest energy of the rotation inversion transitions (23.4 K above ground) (Ho & Townes 1983). The  $\text{NH}_3$ (3,3) image is bright, however, due to a quantum degeneracy in the ‘ortho’ ( $J = 3n$ ) form of  $\text{NH}_3$  which increases its intensity by a factor of two (Ho & Townes 1983). In addition, high temperatures near the Galactic Center make this transition well-populated.

Two assumptions must hold for the method to be valid. First, it is assumed that the two transitions have the same intrinsic linewidth. Our  $\text{NH}_3$ (1,1) and (3,3) velocity integrated maps display a very high degree of correspondence and it seems valid to postulate that the two transitions trace the same material and therefore should have the same intrinsic linewidth. In addition, it is necessary to assume that the opacity does not exceed a particular value,  $\tau_{\text{max}}$ , in either transition. This maximum opacity is used to limit the size of the parameter space which must be searched. In the case below, we have assumed  $\tau_{\text{max}} = 5$  for both  $\text{NH}_3$ (1,1) and (3,3). As seen in §5, almost all points in our dataset have final opacities less than 1.0, which is well below  $\tau_{\text{max}}$ .

The following four steps can be used to recover the intrinsic linewidth and opacity of  $\text{NH}_3$  rotation inversion transitions when observed linewidths and intensities of two transitions are known.

(1) A Gaussian profile is fit to the upper transition, to obtain  $\Delta v_{\text{obs}}$ . This upper transition is chosen because it will be less affected by blending and will give the best initial estimate of  $\Delta v_{\text{int}}$  (see Figure 4b). Using the  $\text{NH}_3$ (3,3) observed linewidth,  $\Delta v_{\text{obs}}(3, 3)$ , the relation between  $\Delta v_{\text{obs}}$  and  $\Delta v_{\text{int}}$  can be used to solve for a range of valid  $\Delta v_{\text{int}}$  corresponding to the case where  $0 < \tau_{\text{m}}(3, 3) < \tau_{\text{max}}$  (see Figure 6c). The range of valid intrinsic linewidths is denoted here as

$$\Delta v_{\text{int,low}} < \Delta v_{\text{int}} < \Delta v_{\text{int,high}} . \quad (6)$$

For example, Figure 6c shows that if  $\Delta v_{\text{obs}}(3, 3) = 15 \text{ km s}^{-1}$  then  $9 \text{ km s}^{-1} \lesssim \Delta v_{\text{int}} \lesssim 14 \text{ km s}^{-1}$  for  $0 \leq \tau_{\text{m}}(3, 3) \leq 5$ .

(2) With a range of valid intrinsic linewidths, the  $\text{NH}_3$ (1,1) observed linewidth,  $\Delta v_{\text{obs}}(1, 1)$ , is used to find the range of acceptable  $\text{NH}_3$ (1,1) opacities. Each curve in Figure 7 corresponds to a different intrinsic linewidth. Therefore Step 1 enables the determination of a range of valid curves where  $\Delta v_{\text{int,low}} < \Delta v_{\text{int}} < \Delta v_{\text{int,high}}$ . There is only a limited range of  $\tau_{\text{m}}(1, 1)$  where the  $\text{NH}_3$ (1,1) observed linewidth lies between the minimum and maximum curves in Figure 7. In this way,  $\Delta v_{\text{obs}}(1, 1)$  is combined with the range of intrinsic linewidths from

Step 1 to calculate a valid range for  $\tau_m(1, 1)$  such that

$$\tau_m(1, 1)_{\text{low}} < \tau_m(1, 1) < \tau_m(1, 1)_{\text{high}} . \quad (7)$$

In the example discussed above, we know  $9\text{km s}^{-1} \lesssim \Delta v_{\text{int}} \lesssim 14\text{km s}^{-1}$ . Now, if  $\Delta v_{\text{obs}}(1, 1) = 30\text{ km s}^{-1}$  then we can use Figure 7 to determine that  $\tau_m(1, 1)$  must lie between 0.9 and 1.9.

(3) The  $\text{NH}_3(3,3)$  opacity can be calculated from the  $\text{NH}_3(1,1)$  opacity and the ratio of the brightness of the main lines of  $\text{NH}_3(3,3)$  to (1,1) using

$$\tau_m(J, K) = -\ln\left[1 - \frac{[\Delta T_A(\nu)]_m(J, K)}{[\Delta T_A(\nu)]_m(1, 1)}(1 - e^{-\tau_m(1, 1)})\right] . \quad (8)$$

As stated in §2, this equation assumes equal beam filling factors and excitation temperatures for  $\text{NH}_3(1,1)$  and (3,3). Given the similarity of the velocity integrated maps for these two transitions (see McGary et al. (2001)), the assumption of equal beam filling factors is reasonable. In addition, the densities of  $10^4 - 10^5\text{ cm}^{-3}$  in these clouds should result in thermalization that will tend to make the excitation temperatures of  $\text{NH}_3(1,1)$  and (3,3) equal. With these assumptions, a range of acceptable  $\tau_m(3, 3)$  can be directly calculated using Equation 8 and the range of  $\tau_m(1, 1)$  found in Step 2 such that

$$\tau_m(3, 3)_{\text{low}} < \tau_m(3, 3) < \tau_m(3, 3)_{\text{high}} . \quad (9)$$

These new limits on  $\tau_m(3, 3)$  provide a tighter constraint than our initial assumption that  $0 < \tau_m(3, 3) < \tau_{\text{max}}$ .

(4) With a smaller range for  $\tau_m(3, 3)$ , we can return to Step 1 and determine a tighter constraint for  $\Delta v_{\text{int}}$ . It follows that this process can be repeated until it converges to a solution for  $\Delta v_{\text{int}}$ ,  $\tau_m(3, 3)$ , and  $\tau_m(1, 1)$  within some predefined tolerance. In our data, we find that the solutions will converge in less than five iterations for a tolerance of 0.4 for  $\tau_m(1, 1)$ . The fast conversion of this method makes it especially useful for datasets with many pixels.

#### 4.1. Estimated Errors

To estimate the error in  $\Delta v_{\text{int}}$  and  $\tau_m$ , we first estimate the error in the fit of  $\Delta v_{\text{obs}}$  to a noisy line profile. Starting with the theoretical line profile,  $I(v, \sigma, \tau_m)$ , noise is added at the 10% level and the observed linewidth,  $\Delta v'_{\text{obs}}$ , is measured. This observed linewidth is

compared to the expected FWHM,  $\Delta v_{\text{obs}}$ , found by fitting a Gaussian to the noiseless profile. The process is repeated until the spread in the differences between  $\Delta v'_{\text{obs}}$  and  $\Delta v_{\text{obs}}$  can be used to estimate the error in observed linewidth. We first model the errors in  $\text{NH}_3(1,1)$  in the case where the channel width is much less than the separation of the hyperfine components. The largest errors (up to  $3 \text{ km s}^{-1}$ ) occur for  $\Delta v_{\text{int}} \approx 5 \text{ km s}^{-1}$  and  $0.5 < \tau_{\text{m}}(1, 1) < 1.0$ . In this case, the five hyperfine components are partially blended, making it difficult to properly estimate a linewidth for the main line. Elsewhere, the expected error in  $\Delta v_{\text{obs}}$  is less than  $0.5 \text{ km s}^{-1}$ . For  $\Delta v_{\text{int}} = 15 \text{ km s}^{-1}$ , the error in the observed linewidth is  $0.3 \text{ km s}^{-1}$  for a spectrum with  $S/N = 10$ . For  $\text{NH}_3(3,3)$ , the hyperfine components have a much smaller effect and the error in the fit to  $\Delta v_{\text{obs}}(3, 3)$  is never greater than  $0.5 \text{ km s}^{-1}$ , independent of  $\Delta v_{\text{int}}$  and  $\tau_{\text{m}}(3, 3)$ .

For the Galactic center data discussed below, the channel width of  $9.8 \text{ km s}^{-1}$  is close to the velocity separation of the hyperfine components and dominates the error for  $\Delta v_{\text{int}} < 5 \text{ km s}^{-1}$ . However, our observations were planned with the knowledge that intrinsic linewidths at the Galactic center range between 10 and  $20 \text{ km s}^{-1}$ . For  $\Delta v_{\text{int}} \gtrsim 5 \text{ km s}^{-1}$ , the fit to  $\Delta v_{\text{obs}}$  is reasonable and the error ranges between 1 and  $2 \text{ km s}^{-1}$  with a slight dependence on  $\tau_{\text{m}}(1, 1)$  and  $\Delta v_{\text{int}}$ . Assuming  $\Delta v_{\text{int}} = 15 \text{ km s}^{-1}$  for the Galactic Center, the  $1\sigma$  error in the fit to  $\Delta v_{\text{obs}}(1, 1)$  and  $\Delta v_{\text{obs}}(3, 3)$  is  $2 \text{ km s}^{-1}$  and  $1 \text{ km s}^{-1}$ , respectively.

Simulations of the error in  $\Delta v_{\text{int}}$  and  $\tau_{\text{m}}(1, 1)$  were made using an error of  $2 \text{ km s}^{-1}$  for  $\Delta v_{\text{obs}}(1, 1)$  and  $\Delta v_{\text{obs}}(3, 3)$  and an error of  $0.01 \text{ Jy beam}^{-1}$  for the amplitude of the  $\text{NH}_3(1,1)$  and  $(3,3)$  main lines. We find a typical error of 0.4 for  $\tau_{\text{m}}(1, 1)$  and  $4 \text{ km s}^{-1}$  for  $\Delta v_{\text{int}}$  with the caveat that the opacities and linewidths cannot be negative. In both cases, errors show a slight increase towards larger values of  $\Delta v_{\text{int}}$  and  $\tau_{\text{m}}(1, 1)$ . This results from the fact that the slope in Figures 6 and 7 becomes more shallow for large values of  $\Delta v_{\text{int}}$  and  $\tau_{\text{m}}(1, 1)$ .

## 5. Results for Galactic Center Data

We have applied the method above to our  $\text{NH}_3(1,1)$  and  $(3,3)$  Galactic Center data for all pixels with calculated linewidths less than  $100 \text{ km s}^{-1}$ . Each pixel was calculated individually and then the resulting map was smoothed with an eight pixel median filter to match the resolution intrinsic to our data. Because pixels for which no value can be determined are set to zero, a convolution by the beam would result in a halo of low values around all features in the map. As a result, every cloud would appear to be optically thin and have low intrinsic linewidths at the edge which could be misleading. The median filter will not produce this halo and is therefore better suited to be used in smoothing the data.

Figure 8 shows the intrinsic linewidth of  $\text{NH}_3$  in the central 10 pc of the Galaxy. The linewidths are in color while a 6 cm continuum emission image (Yusef-Zadeh & Morris 1987) is overlaid in contours. The continuum map shows the outer edge of the expanding SNR, Sgr A East, as well as the ionized arms of the mini-spiral (Sgr A West). Emission associated with the  $2.6 \times 10^6 M_\odot$  supermassive black hole (Eckart & Genzel 1997; Ghez et al. 1998), known as Sgr A\*, is seen as the point source at the center of the map. Previous  $\text{NH}_3(1,1)$  observations of the Galactic Center find  $\langle \Delta v_{\text{obs}}(1,1) \rangle \sim 30 \text{ km s}^{-1}$  for the region (Coil & Ho 1999, 2000), similar to our original results. However, other molecular tracers including  $\text{NH}_3(3,3)$  show significantly smaller linewidths (Güsten & Downes 1980; Armstrong & Barrett 1985). Although the large linewidths in  $\text{NH}_3(1,1)$  are attributed to the nearby hyperfine components, no previous attempt was made to recover the values of the intrinsic linewidths and subsequent calculations of the opacity did not take  $\Delta v_{\text{int}}$  into account. In Figure 8, we have applied our new method, and the average value of  $\text{NH}_3(1,1)$  intrinsic linewidth is  $\sim 15 \text{ km s}^{-1}$ , which is in agreement with that of  $\text{NH}_3(3,3)$  and results from other tracers. *Therefore, we find  $\text{NH}_3(1,1)$  has intrinsic linewidths between 10 and 20  $\text{km s}^{-1}$  in the central 10 pc of the Galaxy.*

At first glance, the  $\text{NH}_3(1,1)$  linewidth appears similar throughout the map. However, there are many details of interest which merit discussion. Readers are referred to McGary et al. (2001) for a more detailed explanation of the locations and morphologies of the features discussed below. Figure 8 shows that most of the gas with  $\Delta v_{\text{int}} > 20 \text{ km s}^{-1}$  is located along the edge of Sgr A East. This shell is expanding into the surrounding molecular material with an energy of  $10^{52}$  ergs, more than an order of magnitude greater than typical supernova remnants (Mezger et al. 1989; Genzel et al. 1990). Recent Chandra observations show a central concentration in the thermal x-rays within the radio shell suggesting that Sgr A East may be an example of a Type II metal rich “mixed-morphology” supernova remnant (Maeda et al. 2001). Emission from the western streamer located on the western edge of Sgr A East at  $(\Delta\alpha = -60'', \Delta\delta = 15'')$  and  $(-70'', -60)$  (McGary et al. 2001) has a typical intrinsic linewidth of  $25 \text{ km s}^{-1}$ , significantly above the average for the region. The  $50 \text{ km s}^{-1}$  giant molecular cloud (GMC), also known as M  $-0.03, -0.07$  (Güsten, Walmsley, & Pauls 1981), is located on the northeastern edge of Sgr A East at  $(100'', 50'')$  and has  $\langle \Delta v_{\text{int}} \rangle \approx 20 \text{ km s}^{-1}$ . Finally, emission at  $(110'', -20'')$  shows  $\Delta v_{\text{int}}$  as large as  $40 \text{ km s}^{-1}$ . These increased linewidths appear to result from the impact of Sgr A East and are a strong indication that these features are in close proximity to the expanding shell (Genzel et al. 1990; Ho et al. 1991; Serabyn, Lacy, & Achtermann 1992; Zylka 1999; Coil & Ho 2000; McGary et al. 2001). The only other cloud with large  $\Delta v_{\text{int}}$  is located at  $(50'', 0'')$  and is less than 2 pc in projected distance from the Galactic Center (assuming  $R_\odot = 8.0 \pm 0.5 \text{ kpc}$  (Reid 1993)). The large intrinsic linewidths in this feature may be due to interactions between multiple

clouds or expansion of the front or back of Sgr A East through the cloud.

The majority of the  $\text{NH}_3(1,1)$  emission is located to the southeast of Sgr A\* and composes the “molecular ridge” that connects the nearby  $20 \text{ km s}^{-1}$  GMC in the south (M  $-0.13, -0.08$ ; Güsten, Walmsley, & Pauls (1981)) to the  $50 \text{ km s}^{-1}$  GMC (Ho et al. 1991; Coil & Ho 1999, 2000; McGary et al. 2001). Previous observations of the southern streamer (from  $(0'', -150'')$  to  $(35'', -75'')$ ) showed an increase in the linewidth as the gas approached the nucleus (Coil & Ho 1999, 2000). After disentangling opacity and linewidth we still see the largest linewidths in the northern edge of this cloud ( $30'', -60''$ ). The large linewidth combined with high temperatures observed in this feature (Coil & Ho 1999) may indicate that the gas is approaching the nucleus. Increased intrinsic linewidths in the southern parts of these clouds may be the result of the impact of a second supernova remnant centered at  $(80'', -120'')$  to the south (Coil & Ho 2000).

When solving for the opacity in the traditional method discussed in §2 we found most gas in our image appeared to have  $1 < \tau_m(1, 1) < 2$ . Although this result is in agreement with Coil & Ho (1999, 2000), it is also contrary to our assumption that all rotation inversion transitions of  $\text{NH}_3$  are typically optically thin at the Galactic Center. Figure 9 shows our result for  $\tau_m(1, 1)$  in color overlaid on 10% contours of  $\text{NH}_3(1,1)$  velocity integrated emission from McGary et al. (2001). After taking the intrinsic linewidth into account using the method described above, the opacity is no longer biased high by the large observed linewidths and  $\langle \tau_m(1, 1) \rangle = 0.6$ . The opacity is highest along the center of the southern streamer (from  $(0'', -150'')$  to  $(35'', -75'')$ ). As seen in Figure 9, the southern streamer is the brightest object in our  $\text{NH}_3(1,1)$  velocity integrated image and is expected to contain  $\sim 5 \times 10^4 M_\odot$  of material (Coil & Ho 1999). This streamer extends northwards from the  $20 \text{ km s}^{-1}$  GMC towards the nucleus (Ho et al. 1991; Coil & Ho 1999, 2000). A second extension of the  $20 \text{ km s}^{-1}$  GMC at  $(-40, -120)$  has  $\tau_m(1, 1) \approx 1$ . The opacity is also elevated in the most northeasterly clump of the  $50 \text{ km s}^{-1}$  GMC. This clump is actually associated with the center of the GMC (to see the full extent of this cloud see Dent et al. (1993)), but is located at the edge of our mosaic where the gain goes to zero (see McGary et al. (2001)). Therefore, the most massive clouds in our maps show the largest opacities as expected.

With these improved estimates of opacity and intrinsic linewidth, the column density and mass could be estimated for each cloud. However, calculation of  $N_{(1,1)}$  requires that the peak antenna temperature of the main line,  $\Delta T_A(1, 1)$ , be measured for each cloud. In addition, to convert  $N_{(1,1)}$  to  $N_{\text{NH}_3}$  the rotational temperature of the gas must be known. Because the objective of this paper is to model the effect of large intrinsic linewidths on the line profile and outline the proper method for determining  $\Delta v_{\text{int}}$  and  $\tau_m$ , these quantities are not presented in this paper. We will present the calculated  $N_{\text{NH}_3}$ ,  $N_{\text{H}_2}$ , and cloud masses in

a subsequent paper focused on the overall environment in the central 10 pc of the Galaxy. For completeness, we present a brief summary of the method to calculate  $N_{(1,1)}$  as well as the average expected value for  $N_{(1,1)}$  in this paper.

The excitation temperature,  $T_{ex}$ , of the gas can be calculated using

$$T_{ex} = 2.7 \text{ K} + \frac{\Delta T_A(1, 1)}{1 - e^{-\tau_m(1,1)}}. \quad (10)$$

This equation assumes a filling factor of 1 and thus produces a lower limit for  $T_{ex}$ .  $T_{ex}$  can then be used to calculate the column density of the main transition using

$$\tau_m(1, 1) = \frac{c^2 h A_{1-0} f(\nu) N_1}{8\pi\nu k T_{ex}} \quad (11)$$

where  $A_{1-0}$  is the Einstein coefficient for spontaneous emission [ $1.67 \times 10^{-7} \text{ s}^{-1}$  for  $\text{NH}_3(1,1)$ ] and  $f(\nu) = (4\ln 2/\pi)^{\frac{1}{2}} (\Delta\nu)^{-1}$  is the line profile for a Gaussian.  $N_1$  is the total number in the upper state and is assumed to be equal to  $N_{(1,1)}/2$  because the inversion doublet is separated by only  $\sim 1$  K. Solving for  $N_{(1,1)}$ , we find

$$N_{(1,1)} = 1.4 \times 10^{14} \text{ cm}^{-2} \tau_m(1, 1) T_{ex} \left[ \frac{\Delta v_{\text{int}}}{10 \text{ km s}^{-1}} \right]. \quad (12)$$

Therefore, we expect clouds to have  $\text{NH}_3(1,1)$  column densities on the order of  $10^{14} \text{ cm}^{-2}$  at the Galactic Center. In this paper, we find that  $\langle \tau_m(1, 1) \rangle = 0.6$  and  $\langle \Delta v_{\text{int}} \rangle = 15 \text{ km s}^{-1}$ . Assuming a lower limit of 7 K for the excitation temperature (Coil & Ho 1999, 2000), we find a lower limit of  $N_{(1,1)} = 8.8 \times 10^{14} \text{ cm}^{-2}$ . Our column density estimate is approximately a factor of five smaller than the typical results of Coil & Ho (1999, 2000), due mostly to the fact that  $\langle \tau_m(1, 1) \rangle$  is smaller throughout the region when the effects of large intrinsic linewidths are removed. As long as the gas is optically thin, the effect of the filling factor on the measured column density is minimized. In this case, small clumps of gas with a large column density is essentially equivalent to gas with a larger filling factor and a smaller column density.

Figure 10 shows that the correlation between  $\tau_m(1, 1)$  and  $\Delta v_{\text{int}}$  after the application of our method resembles a scatter plot. The correlation coefficient is  $-0.14$ , compared to  $0.69$  in Figure 2*b*. By considering the effect of blending, we have successfully modeled the observed linewidth and calculated accurate intrinsic linewidths and opacities. Finally, it is important to note that the spread in  $\Delta v_{\text{int}}$  is very similar to the spread in  $\Delta v_{\text{obs}}(3, 3)$ . Therefore, one may assume that observations of  $\text{NH}_3(3,3)$  give a good indication of the intrinsic linewidth of the gas and corrections need not be applied in general.

## 6. Conclusion

In gas with large intrinsic linewidths, the five quadrupole hyperfine components of the  $\text{NH}_3$  rotation inversion transitions will blend into a single-line profile. The observed linewidth will greatly overestimate  $\Delta v_{\text{int}}$  and bias the opacity to high values. We model the effect of  $\Delta v_{\text{int}}$  on observed  $\text{NH}_3(1,1)$ ,  $(2,2)$ , and  $(3,3)$  linewidths for a range of opacities. A detailed method for recovery of the intrinsic linewidth and opacity using  $\Delta v_{\text{obs}}$  and the intensity of two  $\text{NH}_3$  rotation inversion transitions is then presented. We focus on the case where only the observed linewidth of the profile is known which makes the method particularly useful for correcting historical data for which the exact line profiles are not readily available. Application of this method to our data from the central 10 pc of the Galaxy results in the first independent measures of the opacity and intrinsic linewidth of  $\text{NH}_3(1,1)$  near the nucleus. The calculated intrinsic linewidths when blending is accounted for are reduced by a factor of  $\sim 2$  from the initial observed linewidths to  $\langle \Delta v_{\text{int}} \rangle = 15 \text{ km s}^{-1}$  and now agree with the other molecular tracers in the region, including  $\text{NH}_3(3,3)$ . Gas along the edge of Sgr A East or in close projected distance to the nucleus appears to have increased intrinsic linewidths. All except the most massive clouds in our images show  $\tau_{\text{m}}(1,1) < 1$ . This confirms the observation that even the lowest energy transitions are less affected by self-absorption than  $\text{HCN}(1-0)$  and  $\text{HCO}^+(1-0)$ .

We would like to thank J. Herrnstein and Q. Zhang for helpful comments. RSM is supported in part by a Harvard University Merit Fellowship.

## REFERENCES

- Armstrong, J.T. & Barrett, A.H. 1985, *ApJS*, 57, 535
- Barranco, J.A. & Goodman, A.A. 1998, *ApJ*, 504, 207
- Coil, A.L. & Ho, P.T.P. 1999, *ApJ*, 513, 752
- Coil, A.L. & Ho, P.T.P. 2000, *ApJ*, 533, 245
- Dent, W.R.F, Matthews, H.E., Wade, R. , & Duncan, W.D. 1993, *ApJ*, 410, 650
- Eckart, A. & Genzel, R. 1997, *MNRAS*, 284, 576
- Genzel, R., Stacey, G.J., Harris, A.I., Geis, N., Graf, U.U., Poglitsch, A. , & Sutzki, J. 1990, *ApJ*, 356, 160

- Genzel, R. & Townes, C.H. 1987, ARA&A, 25, 377
- Ghez, A.M., Klein, B.L., Morris, M. , & Becklin, E.E. 1998, ApJ, 509, 678
- Güsten, R., Walmsley, C.M. , & Pauls, T. 1981, A&A, 103, 197
- Güsten, R. & Downes, D. 1980, A&A, 87, 6
- Ho, P.T.P. 1977, Ph.D. thesis, Massachusetts Institute of Technology
- Ho, P.T.P., Ho, L.C., Szczepanski, J.C., Jackson, J.M., Armstrong, J.T. , & Barrett, A.H. 1991, Nature, 350, 309
- Ho, P.T.P., Martin, R.N., Myers, P.C., & Barrett, A.H. 1977, ApJ, 215, 29
- Ho, P.T.P., Martin, R.N., Turner, J.L., & Jackson, J.M. 1990, ApJ, 355, 19
- Ho, P.T.P. & Townes, C.H. 1983, ARA&A, 21, 239
- Maeda, T. et al. 2001, astro-ph/0102183
- McGary, R.S., Ho, P.T.P., & Coil, A.L. 2001, ApJ, 559, 326
- Mezger, P.G., Zylka, R. Salter, C.J., Wink, J.E., Chini, R. Kreysa, E. , & Tuffs, R. 1989, A&A, 209, 337
- Reid, M.J. 1993, ARA&A, 31, 345
- Serabyn, E., Lacy, J.H. , & Achermann, J.M. 1992, ApJ, 395, 166
- Townes, C.H. & Schalow, A.L. 1975, *Microwave Spectroscopy*, New York:Dover
- Zylka, R., Güsten, R., Philipp, S., Ungerechts, H., Mezger, P.G. , & Duschl, W.J. 1999, in ASP Conf. Ser, 186, The Central Parsecs of the Galaxy, ed. H. Falcke et al. (San Francisco: ASP), 415
- Yusef-Zadeh, F. & Morris, M. 1987, ApJ, 320, 545



Table 1. Parameters for NH<sub>3</sub> Rotation Inversion Transitions

| Transition            | Frequency<br>(GHz) | Energy<br>K | Inner Hyperfine                     |                                       | Outer Hyperfine                     |                                       |
|-----------------------|--------------------|-------------|-------------------------------------|---------------------------------------|-------------------------------------|---------------------------------------|
|                       |                    |             | $\Delta v$<br>(km s <sup>-1</sup> ) | Theoretical<br>Intensity <sup>†</sup> | $\Delta v$<br>(km s <sup>-1</sup> ) | Theoretical<br>Intensity <sup>†</sup> |
| NH <sub>3</sub> (1,1) | 23.694495          | 23.4        | 7.7                                 | 0.278                                 | 19.3                                | 0.222                                 |
| NH <sub>3</sub> (2,2) | 23.722633          | 64.9        | 16.5                                | 0.0628                                | 25.7                                | 0.0652                                |
| NH <sub>3</sub> (3,3) | 23.870129          | 124.5       | 21.4                                | 0.0296                                | 28.8                                | 0.0300                                |

<sup>†</sup>Intensity relative to the main line

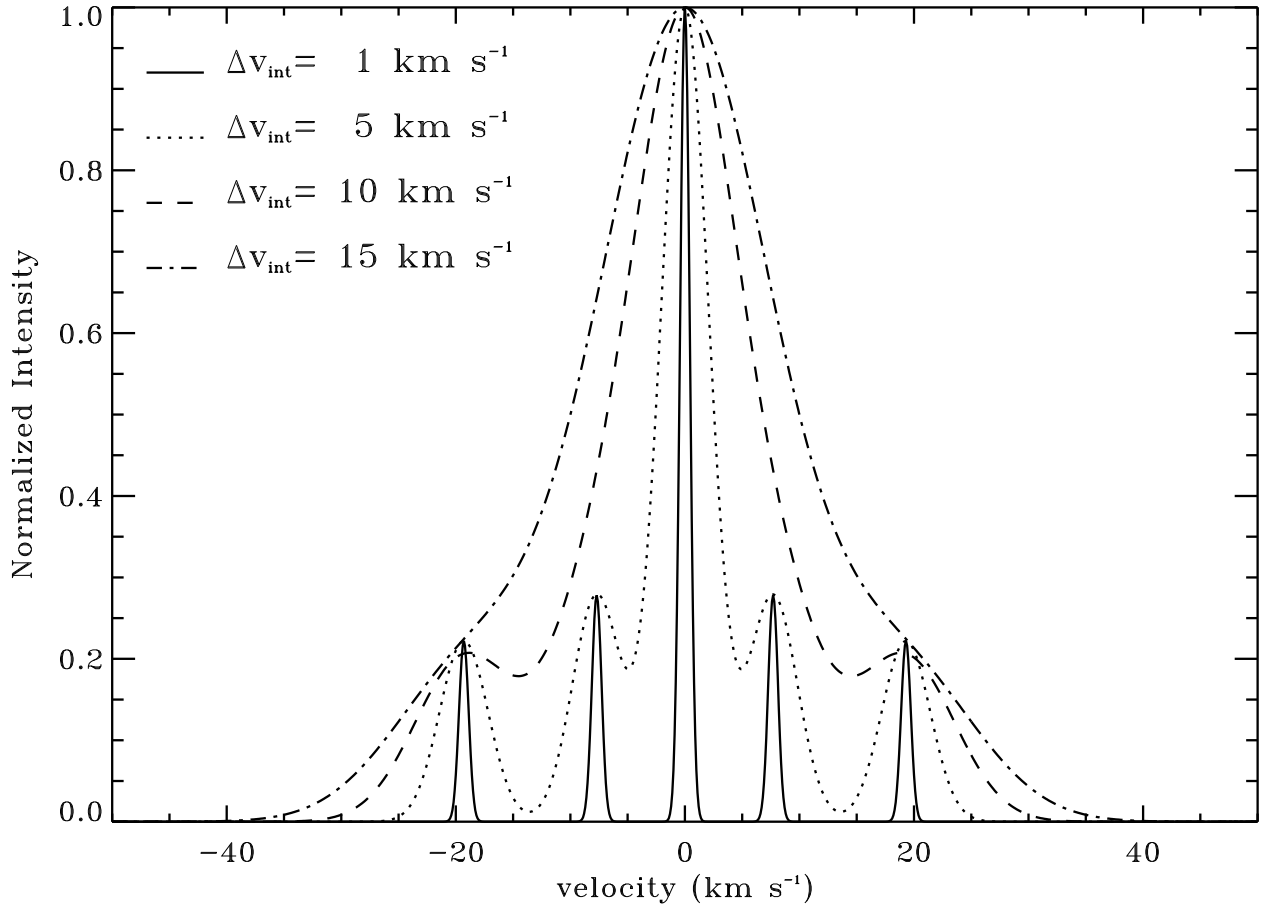


Fig. 1.— Line profiles for NH<sub>3</sub>(1,1) for  $\tau_m \ll 1$  and  $\Delta v_{\text{int}} = 1, 5, 10,$  and  $15 \text{ km s}^{-1}$ . As  $\Delta v_{\text{int}}$  increases, the five electric quadrupole hyperfine components blend into one single line.

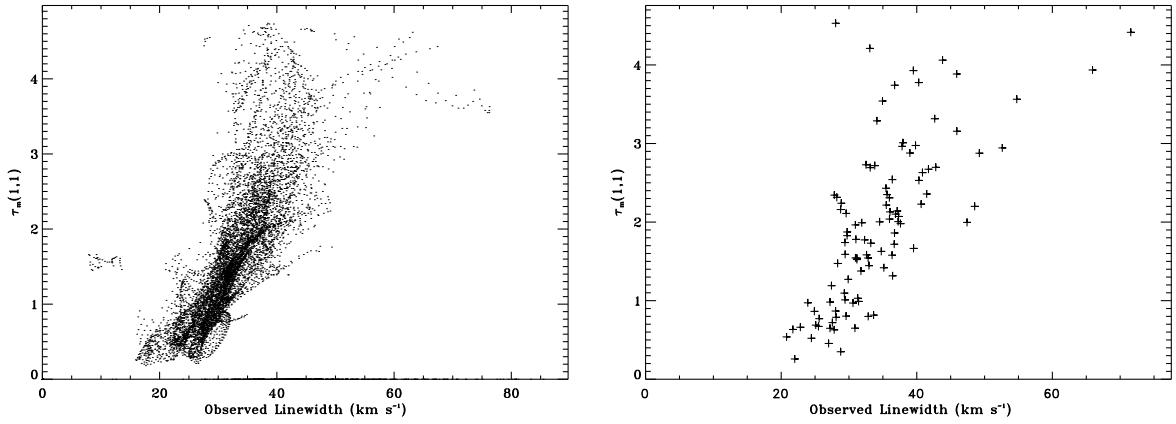


Fig. 2.— *a*) Observed  $\text{NH}_3(1,1)$  linewidth,  $\Delta v_{\text{obs}}(1,1)$ , as a function of  $\tau_{\text{m}}(1,1)$  for all points in our data where the flux was bright enough to fit for both parameters. The strong correlation indicates that blending due to large linewidths has corrupted our results such that an increase in observed linewidth also appears as an increase in opacity. The correlation between adjacent points in the plot is the result of many samplings per beam ( $\theta_b = 15''$ ). *b*) Same as *a*), but the data were first averaged over a single beam and the resulting values for  $\tau_{\text{m}}(1,1)$  and  $\Delta v_{\text{obs}}$  are plotted. The correlation between  $\tau_{\text{m}}(1,1)$  and  $\Delta v_{\text{obs}}$  is still easily observable and has a correlation coefficient of 0.69.

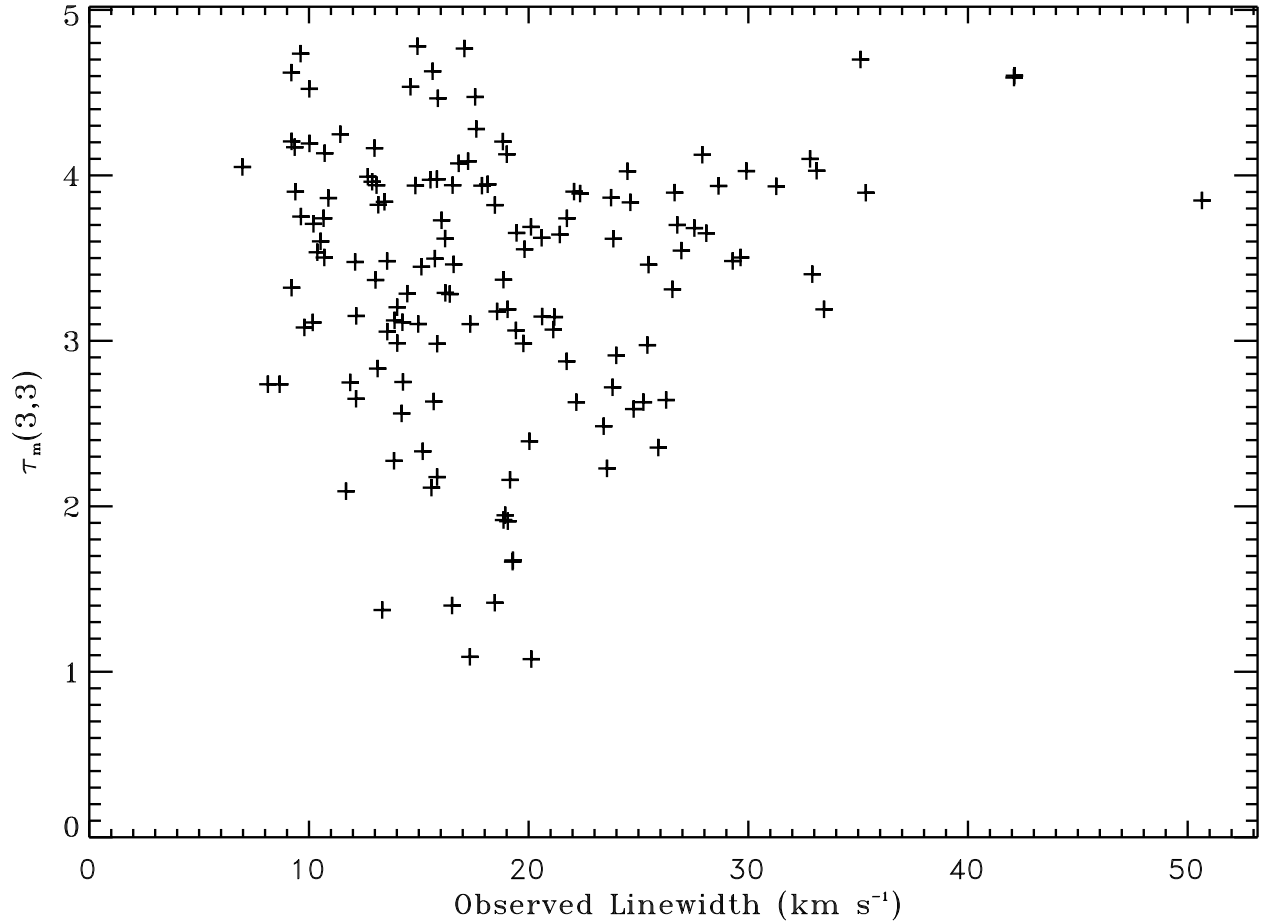


Fig. 3.— Observed NH<sub>3</sub>(3,3) linewidth,  $\Delta v_{\text{obs}}(3,3)$ , as a function of  $\tau_m(3,3)$  for all points in our data where the flux was bright enough to fit for both parameters. The correlation is less strong than in Figure 2 and has a correlation coefficient of 0.07.

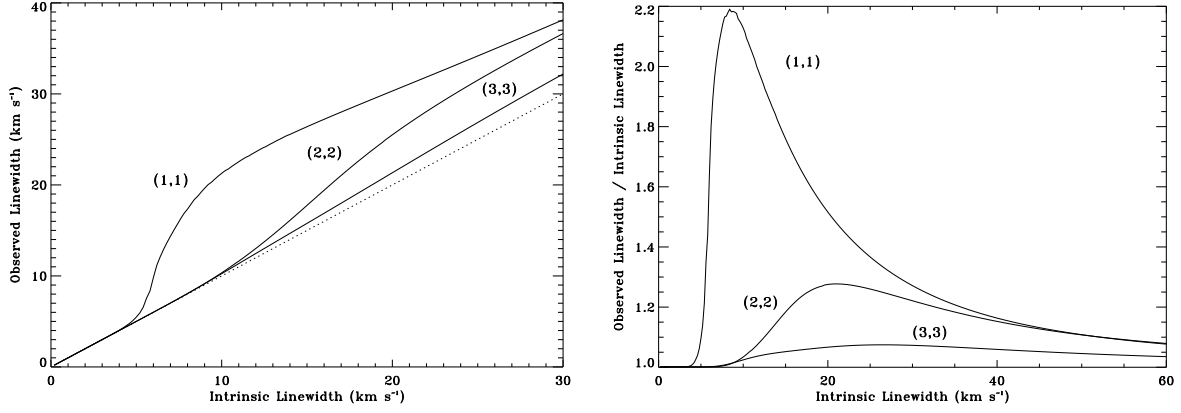


Fig. 4.— *a*) Observed linewidth as a function of intrinsic linewidth for  $\text{NH}_3(1,1)$ ,  $(2,2)$ , and  $(3,3)$  for  $\tau_m \ll 1$ . The dashed line shows  $\Delta v_{\text{obs}} = \Delta v_{\text{int}}$ . Note that the observed linewidth of  $\text{NH}_3(1,1)$  will greatly overestimate  $\Delta v_{\text{int}}$  for  $\Delta v_{\text{int}} > 5 \text{ km s}^{-1}$ . *b*)  $\Delta v_{\text{obs}}/\Delta v_{\text{int}}$  for  $\Delta v_{\text{int}} \leq 60 \text{ km s}^{-1}$  for  $\text{NH}_3(1,1)$ ,  $(2,2)$ , and  $(3,3)$  for  $\tau_m \ll 1$ .

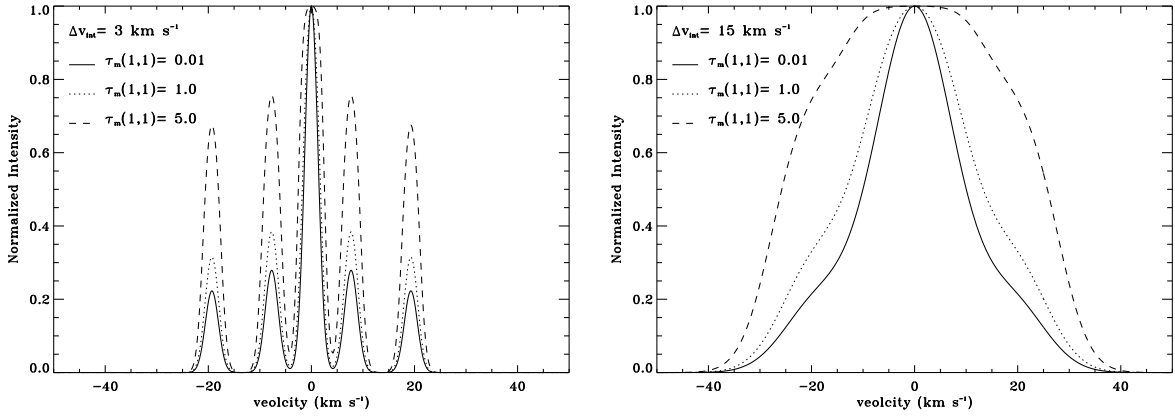


Fig. 5.— *a*) Line profiles of  $\text{NH}_3(1,1)$  for  $\tau = 0.01$ , 1.0 and 5.0 for  $\Delta v_{\text{int}} = 3 \text{ km s}^{-1}$ . In this case, there is no blending so a fit of a Gaussian to the main line will give a good estimate of  $\Delta v_{\text{int}}$  (see Figure 6*a*). *b*) Same as *a*, but for  $\Delta v_{\text{int}} = 15 \text{ km s}^{-1}$ . In this case, the hyperfine components are highly blended and an increase in  $\tau_m(1,1)$  will greatly affect the observed linewidth.

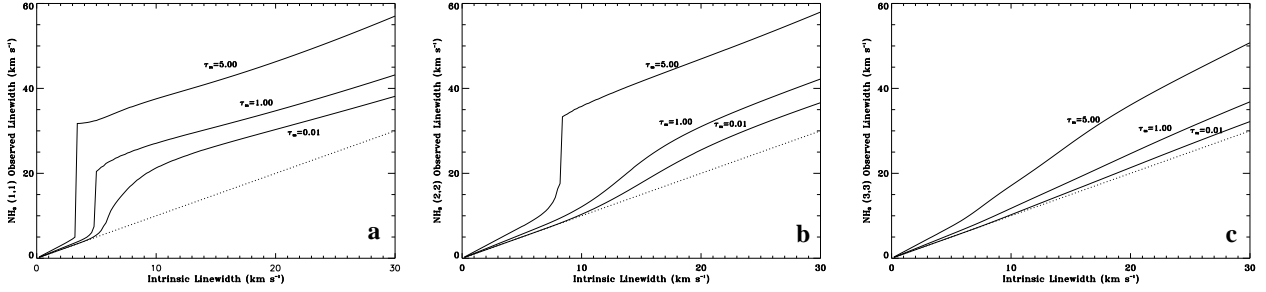


Fig. 6.—  $\Delta v_{\text{obs}}$  as a function of  $\Delta v_{\text{int}}$  for  $\tau_m = 0.01, 1.0, 5.0$  for *a*)  $\text{NH}_3(1,1)$ , *b*)  $\text{NH}_3(2,2)$  and *c*)  $\text{NH}_3(3,3)$ . The dashed line shows  $\Delta v_{\text{obs}} = \Delta v_{\text{int}}$ . For large  $\tau_m$ , a discontinuity develops at  $\sim 3 \text{ km s}^{-1}$  for  $\text{NH}_3(1,1)$  and  $\sim 8 \text{ km s}^{-1}$  for  $\text{NH}_3(2,2)$  where blending of hyperfine lines with comparable intensities suddenly results in a very broad line profile.

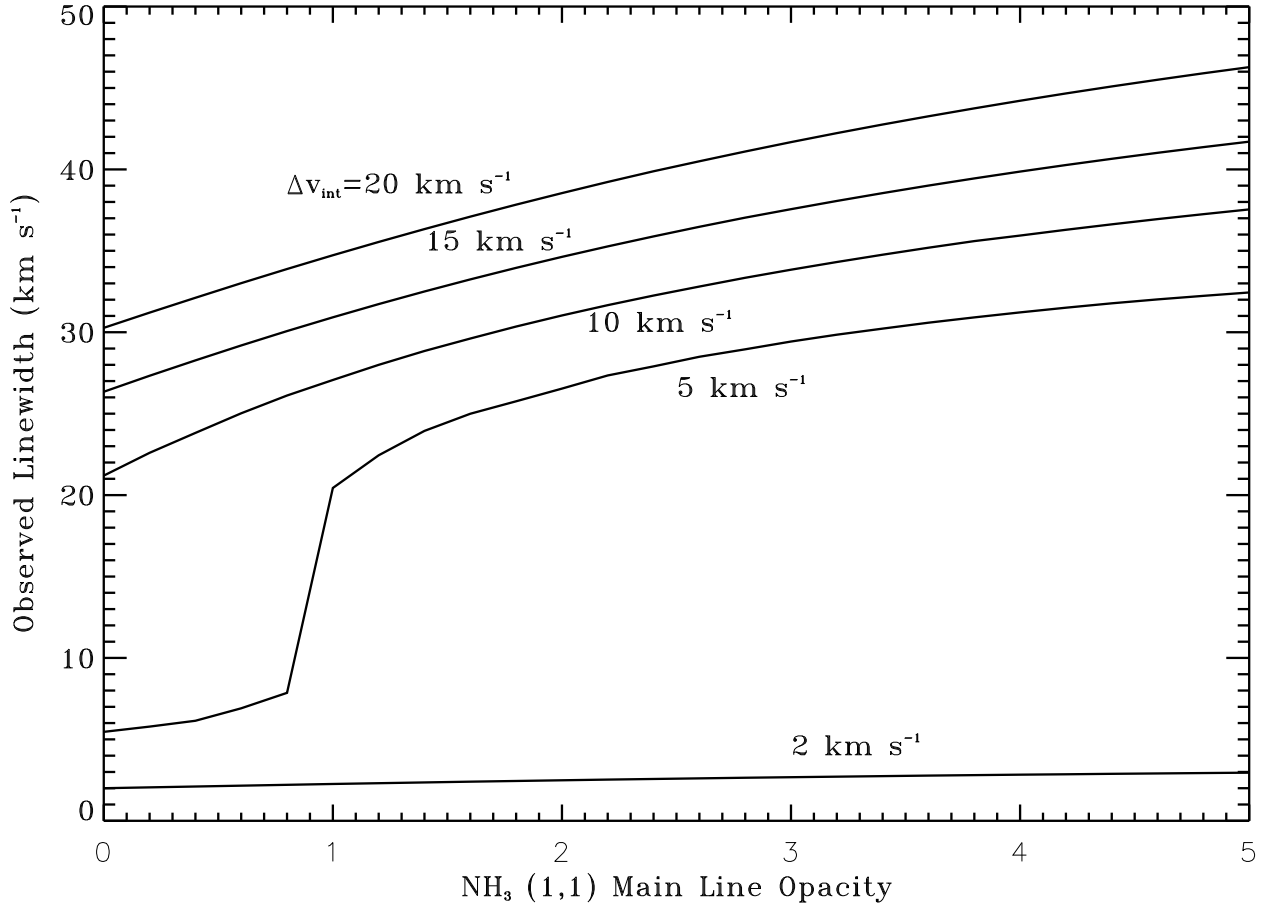


Fig. 7.— Observed  $\text{NH}_3(1,1)$  linewidth as a function of  $\tau_m(1,1)$  for a range of  $\Delta v_{\text{int}}$ .

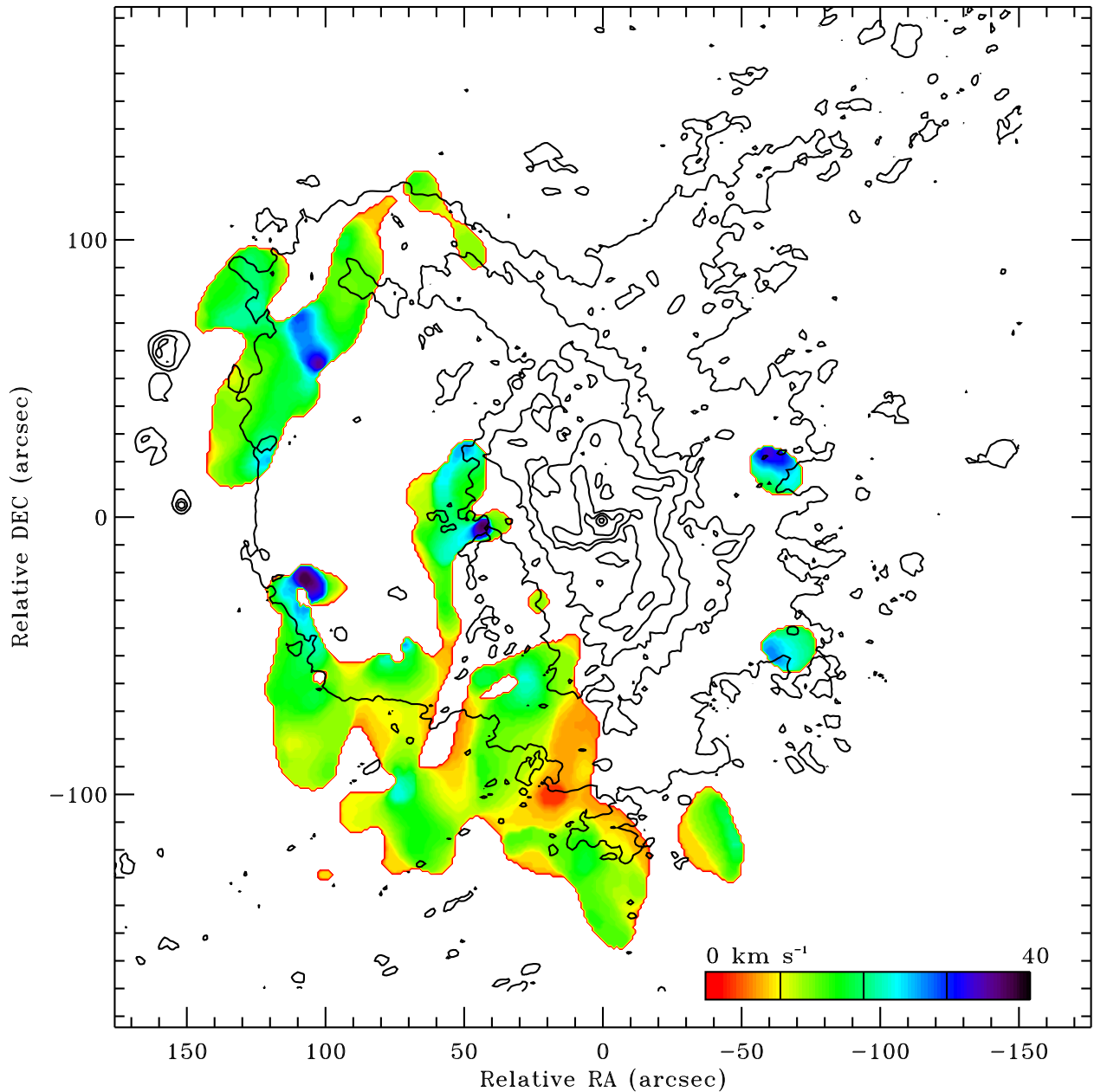


Fig. 8.— Best estimate of  $\Delta v_{\text{int}}$  in color overlaid on an image of 6 cm continuum emission in contours (Yusef-Zadeh & Morris 1987). Contours are 0.001, 0.01, 0.02, 0.04, 0.08, 0.16, 0.32, 0.64, and 1.28  $\text{Jy beam}^{-1}$ . The linewidth map has been smoothed with an eight pixel median filter (see §5). The continuum image shows the location of the expanding shell, Sgr A East, the mini-spiral, and Sgr A\*. Typical intrinsic linewidths are 15  $\text{km s}^{-1}$ . The largest  $\Delta v_{\text{int}}$  appear to be located near the nucleus or on the edge of Sgr A East.

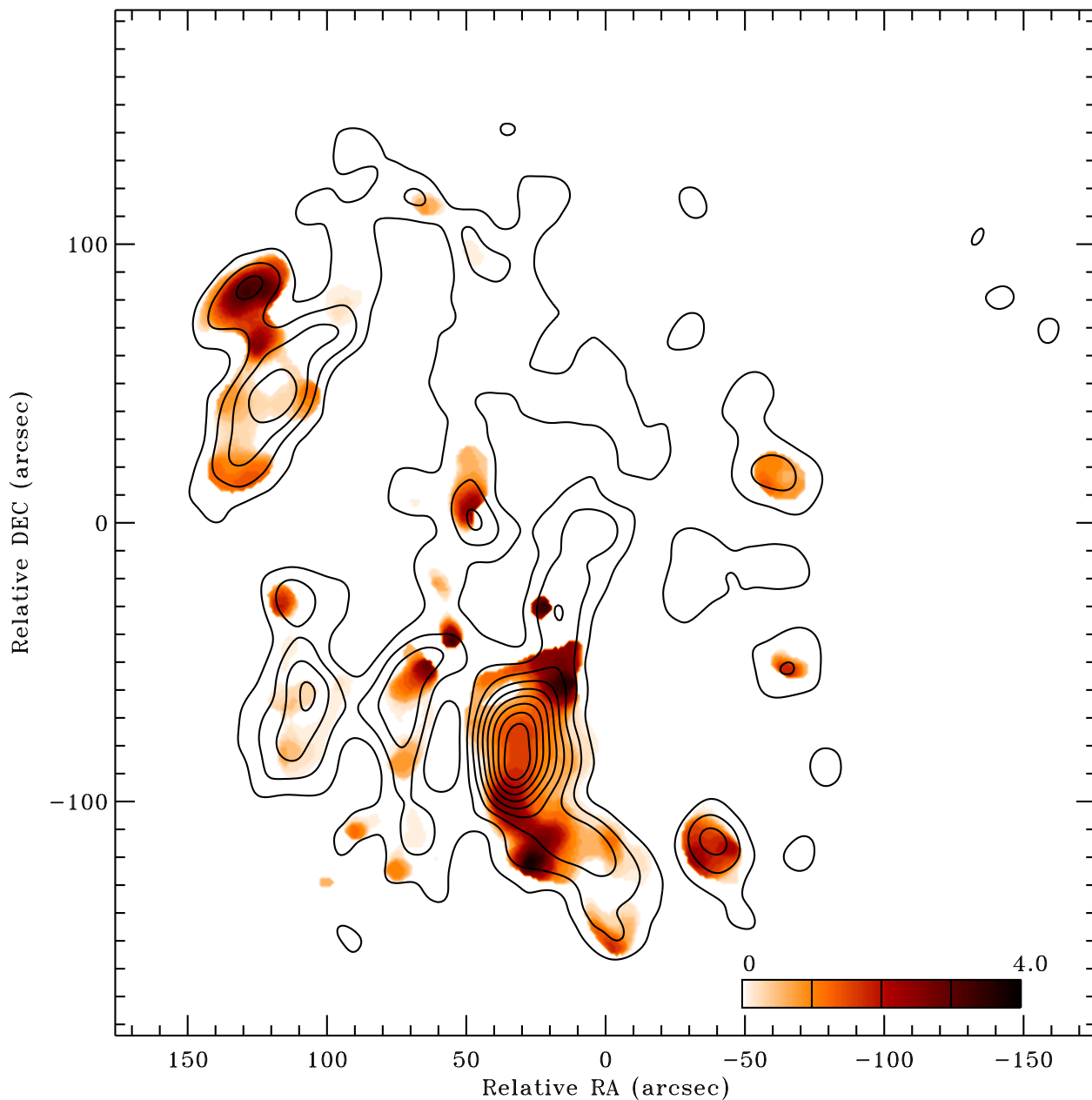


Fig. 9.— Best estimate of  $\tau_m(1,1)$  in color overlaid on velocity integrated  $\text{NH}_3(1,1)$  emission in 10% contours (McGary et al. 2001). The opacity map has been smoothed with an eight pixel median filter (see §5). The highest opacity is associated with the southern streamer and the 20 and 50  $\text{km s}^{-1}$  GMCs while most other features have  $\tau_m(1,1) < 1.0$ .



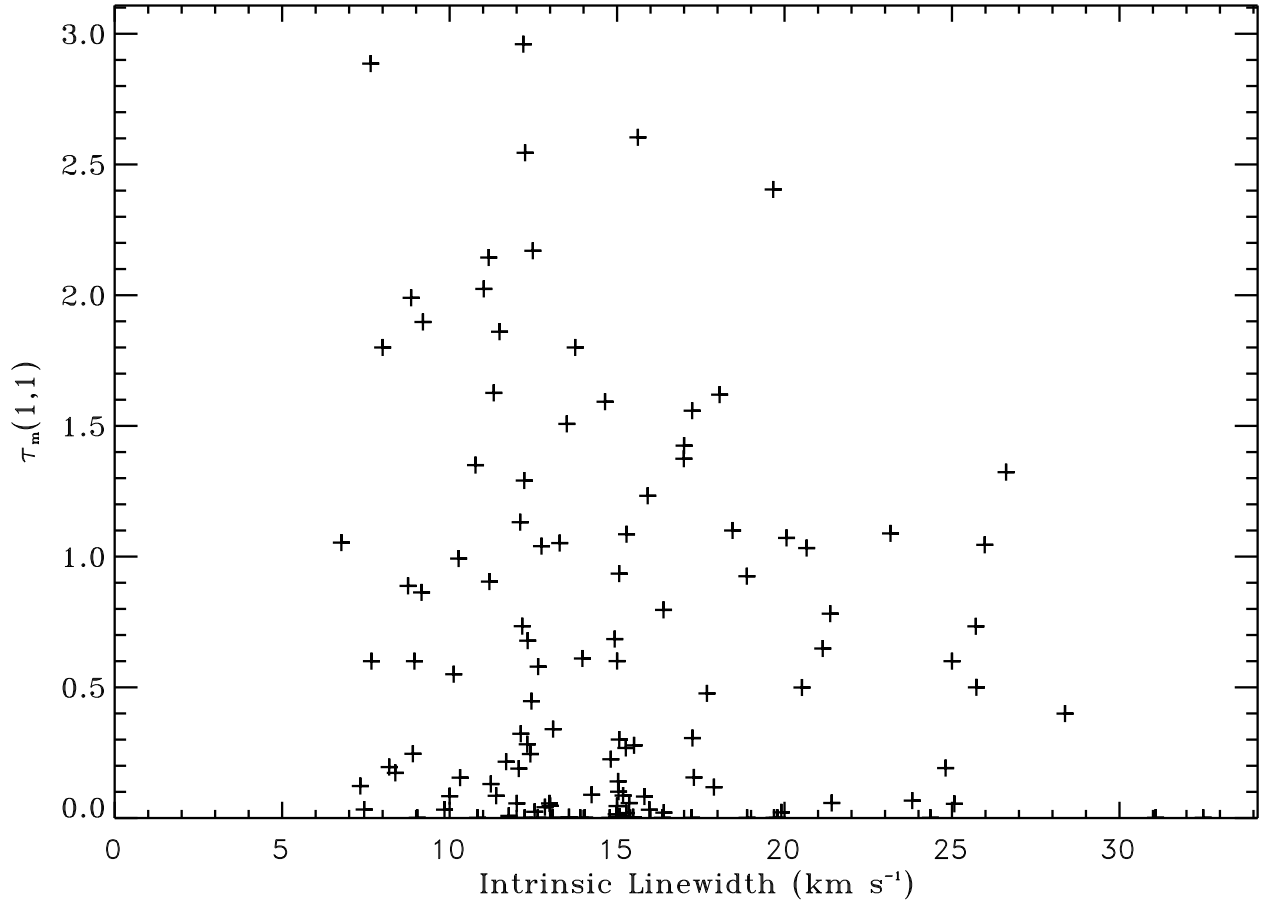


Fig. 10.— Intrinsic linewidth,  $\Delta v_{\text{int}}$ , as a function of  $\tau_m(1, 1)$  after application of our correction method. Averages over the 15'' beam have been taken as in Figure 2*b* and the correlation coefficient is only -0.14.